THE $^{12}C(N, 2N)^{11}C$ CROSS SECTION FROM THRESHOLD TO 26.5 MEV

Mark Yuly, Ian Love, Garrett Hartshaw, Houghton College, Houghton, NY USA

Stephen Padalino, Megan Russ, Mollie Bienstock, Angela Simone, Drew Ellison, Holly DeSmitt, State University of New York at Geneseo, Geneseo, NY USA

Thomas N. Massey, Ohio University, Athens, OH USA

Craig Sangster, Laboratory for Laser Energetics, Rochester NY USA.

INTRODUCTION

Tertiary neutrons, produced by energetic knock-on tritium and deuterium ions in the nuclear fuel of an inertial confinement fusion implosion, can be used as a diagnostic tool for characterizing the DT fusion reaction. A robust technique for measuring the number of tertiary neutrons released may be $^{12}C(n, 2n)^{11}C$ activation of graphite samples placed within the reaction chamber. The high threshold for this reaction, at 20.295 MeV, means this technique will be insensitive to the 14 MeV primary neutrons released in the DT fusion reaction, but still sensitive to tertiary neutrons which can range in energy from 14 MeV up to as high as 30 MeV. The $^{12}C(n, 2n)^{11}C$ cross section is needed in order to calculate the number of tertiary neutrons from the amount of ^{11}C produced in the graphite sample. Unfortunately, this cross section is not well measured. From Figure 1, which shows all known measurements [1-7] for the $^{12}C(n, 2n)^{11}C$ cross section, it is clear that previous measurements vary by as much as a factor of two in the energy region from threshold up to 30 MeV. Even near threshold, where the measured cross section curves converge, the cross sections still do not agree. While all of the previous experiments were activation measurements, there does not appear to be any obvious trend based on type of neutron source, type of target, method used to measure the neutron flux or type of activation measurement.

During the summer of 2012 an experiment was performed to study the feasibility of measuring the $^{12}C(n,2n)$ cross section at the Ohio University Accelerator Laboratory using the 4.5 MV Tandem Van de Graaff accelerator. This was followed in 2013 by a more complete measurement up to 26.4 MeV, the maximum energy reachable using the tandem accelerator. In this experiment, the number of ^{11}C nuclei produced by monoenergetic neutrons striking polyethylene and graphite targets were counted by detecting the back-to-back positron annihilation 0.511 MeV gamma rays in coincidence with NaI detectors. The neutron flux was measured using proton recoil from the polyethylene target into a dE-E silicon detector telescope.

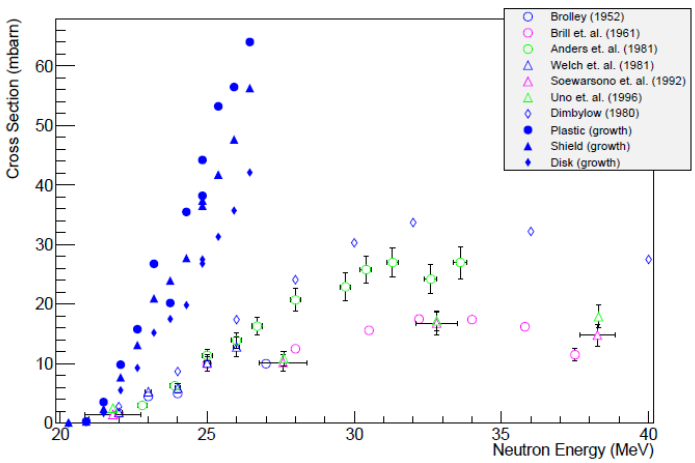

Figure 1. Previous and current experimentally measured and calculated cross sections [1-7] for $^{12}C(n, 2n)^{11}C$. Very preliminary results for the present measurement using the polyethylene target (red circles), graphite target (red diamonds) are shown. Statistical error bars are smaller than symbols for current measurements.

Preliminary results for this experiment and with only preliminary values for the NaI detector efficiencies are also shown in Figure 1. The preliminary results have the correct order of

magnitude, the predicted increasing trend with incident neutron energy, and the threshold is where it was expected. However, the overall normalization is not yet known.

EXPERIMENT

The cross sections were measured for energies between about 19.7 and 26.4 MeV using the 4.5 MV Tandem van de Graaff accelerator at Ohio University. Figure 2 shows the activation set up. Deuterons were accelerated to energies between 3.1 and 9.1 MeV and allowed to strike a 12.78 μCi tritium target, shown in Figure 3, located in the end of the beam pipe just upstream of an aluminum end window. Deuteron beam currents were typically between 0.8 and 1.0 μA. The tritium was deposited as titanium tritide on a 49 mm diameter 1 mm thick OFHC copper substrate at a density of about 2000 $\mu g/cm^2$ over a circular active area of 30 mm diameter. The end window was cooled by a stream of air and the end of the beam line, including the target, was moved in a circular path by the "wobbler" to keep the beam from overheating any one place on the target.

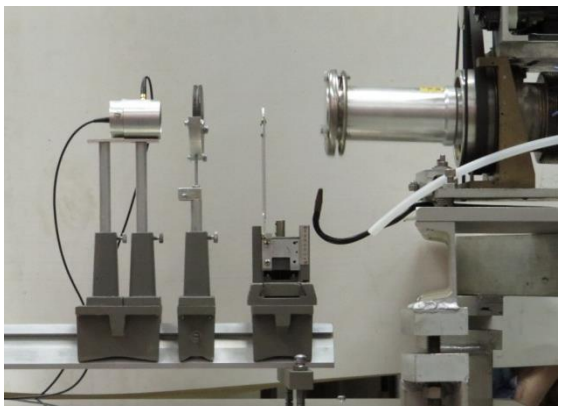

Figure 2. The activation setup. Beam deuterons hit the tritium target just inside the end of the beam line. Neutrons produced in the $^3H(d,n)^4He$ reaction then hit the polyethylene and graphite targets. The detector telescope measures the rate of elastic np scattering.

Before striking the target, the deuteron beam was defocused by a pair of quadrupole magnets located 275 and 315 cm upstream, and allowed to pass through a 1.27 cm diameter collimator 45 cm upstream of the target.

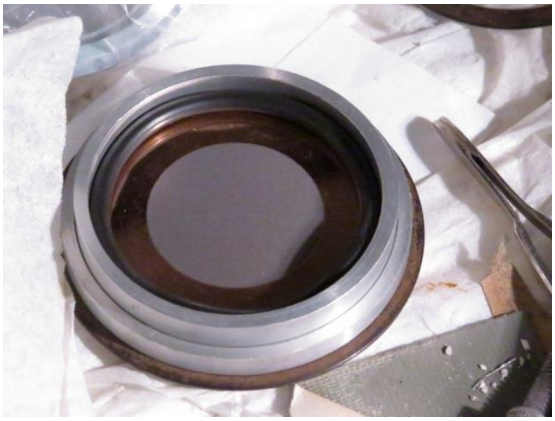

Figure 3. The tritium tritide target prior to insertion into the beam.

This was to ensure that the beam filled the collimator and therefore that the beam spot on the target was relatively large to reduce heating and always struck the target at the same known location.

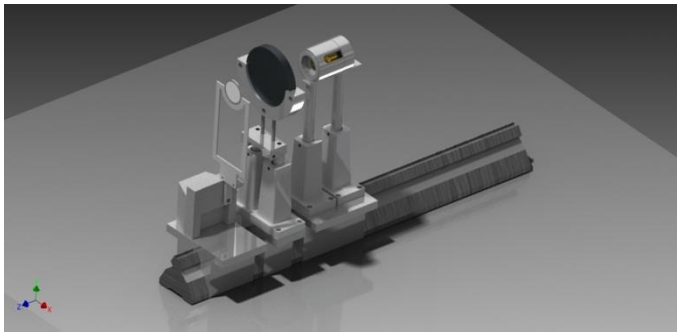

Figure 4. CAD drawing of the new target and detector holder, consisting of an optical bench and modified positioners.

The system used for positioning the targets and detectors during the summer of 2012 had several disadvantages that were addressed during the 2013 experiment. The 2012 apparatus was designed to minimize the amount of material near the targets and around the detector in order to reduce background. Analysis later revealed that the background was relatively small, and a sturdier holder that allowed for more convenient alignment and reproducible positioning could be substituted. Figure 4 shows the 50 cm long optical bench with modified positioners that was used to position the polyethylene and graphite targets, and to hold the

detectors in fixed positions at an angle of 0° with respect to the beam.

Neutrons leaving the neutron source were allowed to strike a 1.64 mm thick, 2.54 cm diameter high-density polyethylene target located 7.0 cm from the tritium target and a 7.62 cm diameter 0.89 cm thick disc of high purity graphite with a 17.46 mm hole drilled in through its center 14.4 cm from the tritium target. Upstream of the graphite target a pair of graphite shield disks stopped protons scattered from the polyethylene from reaching the graphite target. The two shields, one 1.28 mm and the other 2.57 mm thick, were graphite disks with the same diameter as the graphite target.

A proton telescope, shown in Figure 5, consisting of a 300 µm thick, 150 mm^2 ion implanted silicon ΔE detector and a 5000 µm thick, 200 mm^2 drifted-lithium silicon E detector was placed behind the hole in the graphite target, so that protons coming from the polyethylene could be viewed. The entrance of the ΔE detector was covered by a 0.005 mm thick aluminum foil to keep out ambient light. The entire detector assembly was housed in an aluminum tube with wall thickness of about 2.9 mm and diameter of 3.47 cm. Preamplifiers and spectroscopy amplifiers located near the detectors in the experimental hall sent pulses to a FastComTech MPA-3 multiparameter system which digitized and recorded the pulse heights and timing. The system also recorded the deuteron beam current.

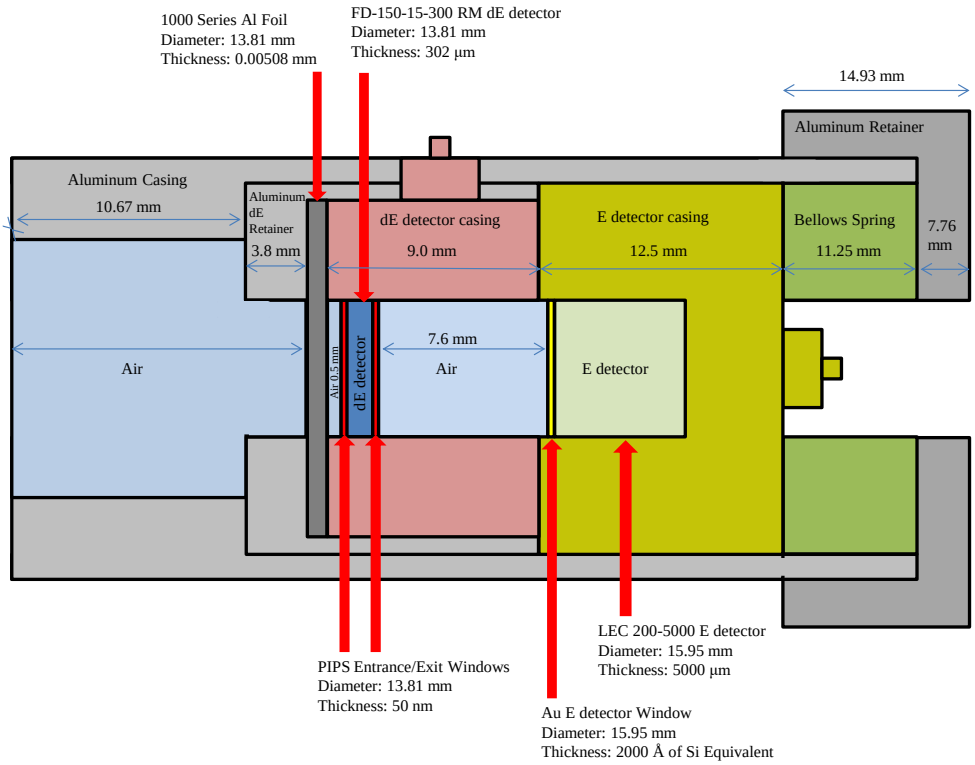

Figure 5. Schematic diagram of proton telescope.

Figure 6 shows 2D histograms of the pulse height in the dE detector versus the E detector. The left histogram shows the results with 26.4 MeV neutrons hitting a 1.64 mm thick 2.54 cm diameter polyethylene target, while for the right histogram the target holder is empty. The protons elastically scattered from the polyethylene can be easily identified by their energy loss in the two detectors.

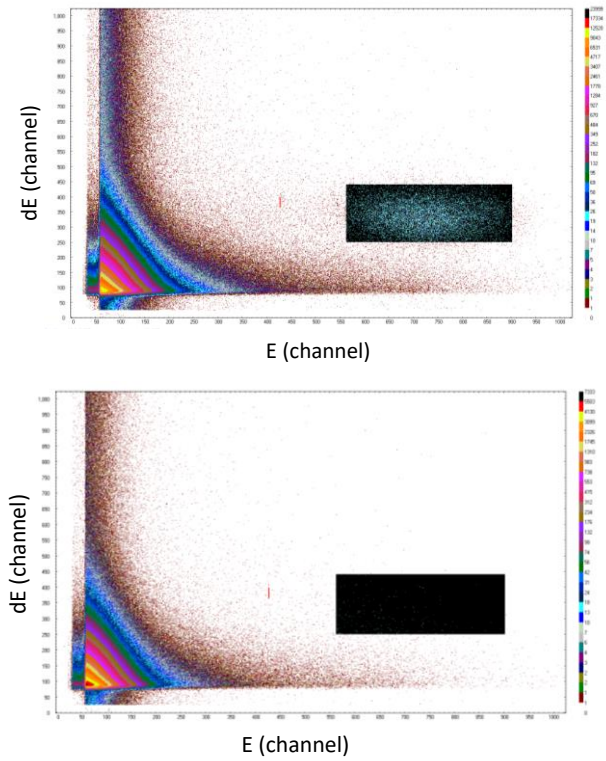

Figure 6. (Top) Histogram of dE versus E for 26.4 MeV neutrons striking the polyethylene target. The proton island is clearly visible. The marked region-of-interest indicates the protons counted as elastically scattered by neutrons. (Bottom) Same but with the polyethylene target removed.

At 26.4 MeV the background count rate was about 3% of the rate with the polyethylene target in place, which was approximately 3.5 protons/sec with a beam current of about 1 μA. Over the course of the experiment, radiation damage caused the width of the proton peak in the E detector to gradually increase along with the leakage current.

A 5 inch diameter liquid scintillator neutron monitor was located 300 cm from the tritium target at an angle of a 71.4° to beam left. In order to identify neutron pulses from gammas, a pulse shape analysis was made using a Mesytec MPD4 pulse shape discriminator module, which produced analog outputs proportional to the amplitude and width of the pulses from the neutron monitor photomultiplier. These signals were input into the MPA-3 multiparameter system, which caused the problems described below.

For this measurement it was very important that the beam was aligned with the central axis of the targets and detectors, and that the beam spot did not move on the tritium target as the energy was changed.

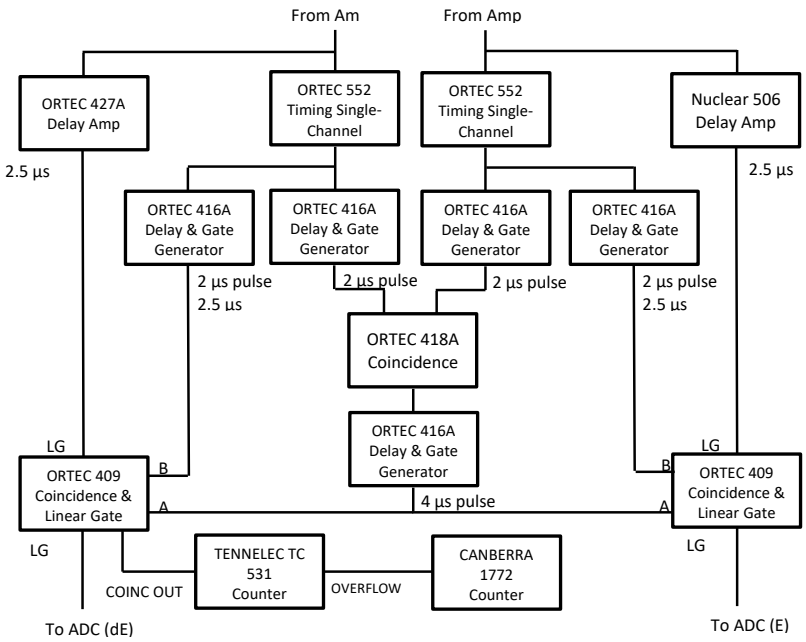

Figure 7. Pulses from the dE and E silicon detectors are hardware gated by the requirement that they be above a set threshold and be in coincidence before they are allowed into the ADC. This circuit allows an external count of the number of coincidence events permitting an independent determination of the dead time to be made.

As a check, prior to each activation run at a new energy the rate of detecting elastically scattered protons was measured as a function of the current in the last quadrupole focusing magnet. If the beam passed through the center of the magnet, changing the current would only result in defocussing the beam on the collimator, and the proton rate as a function of current on the tritium target or counts in the neutron monitor would not change. When this was carried out, however, the behavior of the proton rates led to a closer examination of the dead time for the experiment.

The circuit shown in Figure 7 was created in order to provide a hardware count of the number of coincidence events, as well as to gate the individual detector pulses using a separate hardware discriminator to control the thresholds. Logic pulses from timing single channel analyzers (TSCA) triggered on the analog pulses from the dE and E detectors were input to gate generators to create 2 μs logic pulses to form a dE-E coincidence. They also were used to create 2.5 μs wide logic signals to gate in the linear gates the delayed analog pulses from the detectors. These linear gates were only allowed pass the analog signals when they occurred within 4 μs of the coincidence between dE and E. By comparing the number of coincidence events recorded by the computer with the number counted by the visual scaler, the live time could be calculated.

Using this independent technique for measuring the dead time, it was possible to determine that the neutron monitor signals going into the MPA-3 were causing the dead time for the entire system to be very high – although the computer reported the dead time to be around 10-15%, the actual dead time was about 80% when the neutron monitor was plugged in. Disconnecting the neutron monitor signals caused the dead time to fall to a few percent, and the dead time reported by the computer came into agreement with the dead time calculated by hand using the visual scaler.

A separate circuit, shown in Figure 8, was then set up to count the number of high energy neutrons detected by the neutron monitor. The Mesytec MPD4 pulse shape discriminator outputs a pulse proportional to the amplitude of the signal from the liquid scintillator and a TAC signal which is proportional to the pulse width. By using the timing single channel analyzer (TSCA) to only produce a gate for the largest pulses, and delaying the TAC signal with a delay amplifier to arrive simultaneously with the gate, the plot in the lower figure was obtained. This plot shows that for large amplitude pulses, gamma rays and neutrons have different pulse widths, and allows only the high energy neutrons (blue region) to be counted.

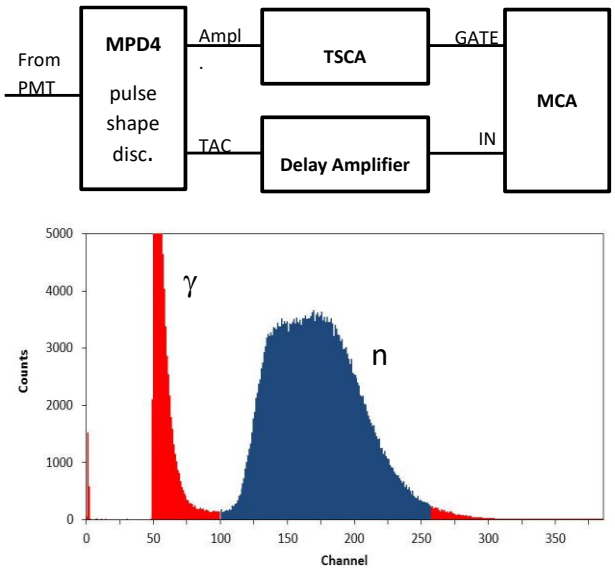

Figure 8. Circuit for neutron monitor pulse height analysis (top) and pulse shape analysis spectrum (bottom). Pulses with large amplitudes and wide pulse widths are result from high energy neutrons (blue region).

Activated targets were counted at three counting stations located in an adjacent room, shown in Figure 9. After each was activated simultaneously, the graphite, shields and polyethylene targets were placed between pairs of 3 inch diameter by 3 inch thick NaI detectors. Coincidence events consisting of two back-to-back 0.511 keV gamma rays from

positron annihilation could be selected and counted as a function of time. This allowed the growth curve of ^{11}B to be measured and fit in order to determine the number of ^{11}C nuclei present. Pulses from all of these detectors were sent to a FastComTech MPA-4 system, which recorded the pulse heights and timing information.

Preliminary efficiencies for the NaI detectors were determined. Table 1 shows the singles and coincidence efficiencies for the geometries of the targets used in the experiment.

Figure 9. Three counting stations were used for the graphite target, the polyethylene target, and the graphite shields. Positron annihilation gamma rays detected in coincidence were digitzed and recorded using an MPA-4 multiparameter system.

Table 1. Calculated efficiencies for the NaI detectors for the graphite disk, shield and polythene target geometries for singles and coincidence configurations.

Target	Singles Efficiency (%)	Coincidence Efficiency (%)
Graphite Disk	6.03	0.86
Shields	6.38	0.91
Plastic	7.85	1.95

PROCEDURE

The detector and targets were first positioned at 0° using a downstream optical telescope that had been previously aligned with the collimator in the beam pipe and monuments in the target room. The position of the optical bench was set by using a plumb bob with a string running directly down the cap on end of the beam line, just downstream of the tritium target. The plumb bob was used to position the optical bench so that the end cap was located at the 5 mm mark on the optical bench scale, so that zero corresponded to the location of the tritium target.

For each energy setting, prior to activating the targets a study was made of the positioning of the beam in the beam pipe. This is important because a small change in the position of the beam spot on the tritium target had a large effect on the scattering angles and therefore the count rates. In order to ensure proper alignment of the beam, the current in the last quadrupole magnet just before the collimator was changed. Any displacement from the central axis of the beam pipe would then cause the beam spot to move, which could be detected by carefully monitoring the number of protons per integrated charge and the ratio of protons to neutrons detected in the neutron monitor. Figure 10 shows a typical scan in which the ratios were measured to less than 5% statistical uncertainty.

Following the quadrupole tests, a shield, graphite target and a polyethylene target were placed in the target holders to be activated for about 1.5 hours. Three identical sets of targets were available to be used consecutively in order to allow enough time for any longer lived activated contaminants to decay, although none were detected. When the deuteron beam was stopped, after sufficient time to allow the radiation dose rate to fall to an acceptable level, the targets were hand-carried to the counting room and placed in the counting stations.

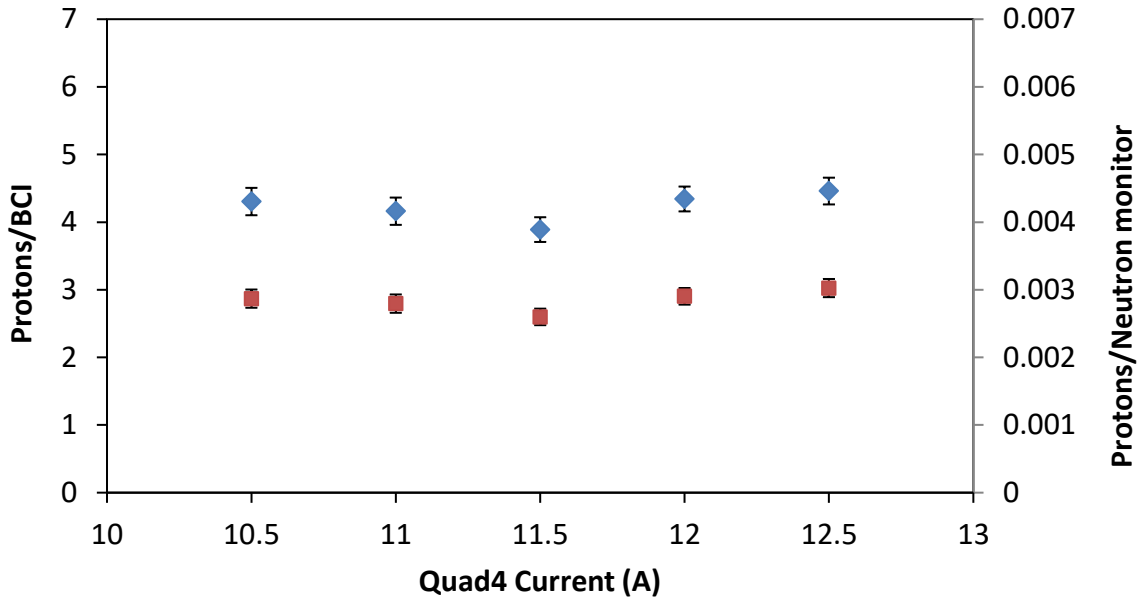

Figure 10. Prior to each activation measurement, the proton/total integrated charge (blue) and proton/neutron monitor counts (red) ratios were measured as a function of the current in the last quadrupole magnet. If the beam is aligned properly, these ratios should not change.

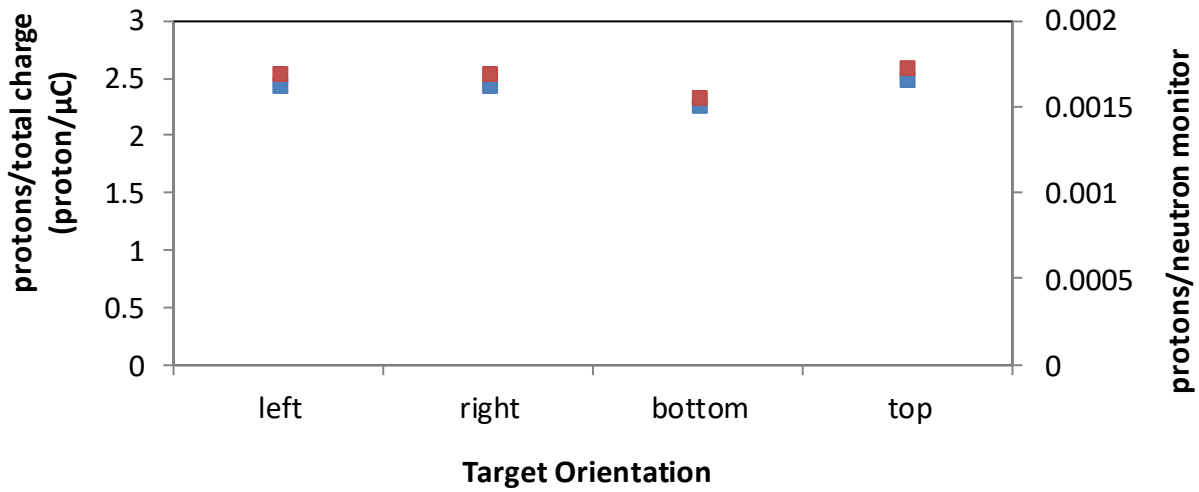

Figure 11. Protons/integrated charge (blue) and protons\neutron monitor counts (red) for the half polyethylene target rotated to four orientations. For perfect alignment these ratios should remain constant. Error bars are smaller than the symbols.

The time between when irradiation stopped and when target counting commenced was recorded, and was typically around 4-5 minutes. Each sample was then counted for approximately 2 hours, with the rate binned into 50 second intervals. The dead time for each time bin is recorded and used to correct the growth curve.

The number of background protons was measured at each energy setting by removing the polyethylene target and counting for approximately

30 minutes. A special graphite disk and polyethylene target was used exclusively for this purpose.

Several other tests were also performed. A polyethylene target was cut in half and the proton count rate was measured to approximately 2% statistical uncertainty for the target in each of four positions. The target position was changed by simply rotating it in the holder. The results, which are shown in Figure 11, are not quite constant, which is what would be expected for the complete symmetry present if the system is perfectly aligned along 0° and the beam spot is perfectly uniform. The rate is slightly lower when the plastic was filling the bottom half. This may mean that the target was slightly higher than the beam line or that the beam spot was high, or that it was non uniform.

ANALYSIS

In order to determine the cross section for the ^{12}C(n, 2n) reaction from the number of ^{11}C decays counted in the counting station and the number of np elastically scattered protons counted using the proton telescope, the easiest way to proceed is to make some simplifying assumptions, namely, that the tritium and polyethylene targets behave as point sources for neutrons and protons, respectively, as shown in in Figure 12.

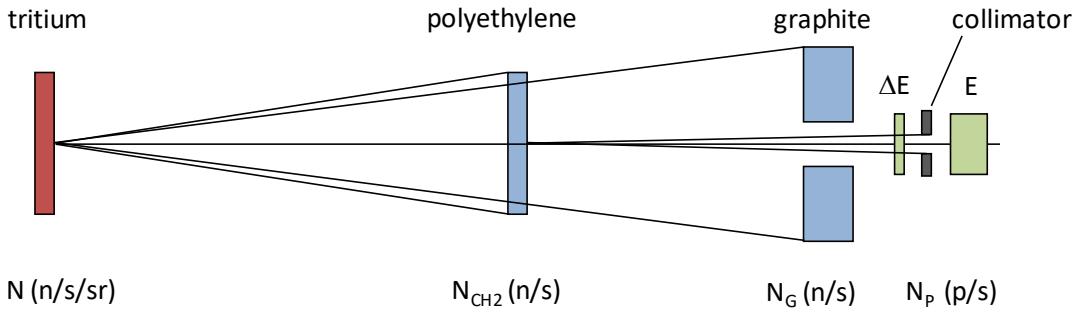

Figure 12. A schematic diagram used for initial estimates of the cross section. The tritium and polyethylene targets are treated as point sources for neutrons and protons, respectively.

Assume that the tritium target is an isotropic point source of monoenergetic neutrons with flux *N* (neutrons/sec/sr). In that case, the number/sec of neutrons on the polyethylene (N_{CH2}) and graphite (N_G) targets would be given by

$$\boldsymbol{N_{CH2} = N\Omega_{CH2}} \text{ and } \boldsymbol{N_G = N\Omega_G} \qquad (1)$$

where Ω_{CH2} and Ω_G are the solid angles of the plastic and graphite targets, respectively, if the effect of the finite thickness of the targets on solid angle is neglected. The number of protons/sec (N_P) detected by the proton telescope can be easily obtained if the polyethylene target is treated as a point source for the purpose of scattering protons into the proton telescope. Assuming that the cross section for np elastic scattering (σ_{np}) is constant over the angles subtended by the targets, and is equal to the cross section at 0°, yields

$$\boldsymbol{N_P = \sigma_{np}(0°)\, T_H N_{CH2} \Omega_P} \qquad (2)$$

where $T_H$is the thickness (in number of hydrogen nuclei/area) of the polyethylene target, and Ω_P is the solid angle of the proton telescope. From this, we see that the ratio of neutrons hitting the plastic target to protons detected by the proton telescope, in this simple approximation, is given by

$$\frac{N_{CH_2}}{N_p} = \frac{1}{\sigma_{np} T_H \Omega_p}. \qquad (3)$$

Now consider the ^{12}C(n, 2n) reaction occurring in the plastic and graphite targets. The number of ^{11}C nuclei is changing because ^{11}C nuclei are being created and at the same time ^{11}C nuclei are decaying. The rate the number of ^{11}C nuclei (N_{C11}) changes is given by

$$\frac{dN_{C11}}{dt} = \sigma T_C N_{CH2} - \lambda N_{C11} \quad (4)$$

where $\sigma T_C N_{CH2}$ is the rate ^{11}C is being created and λN_{C11} is the decay rate. Here σ is the ^{12}C(n,2n)^{11}C total cross section and T_C is the areal density of carbon nuclei in the polyethylene target. Solving this differential equation for the cross section yields

$$\sigma = \frac{N_{C11}}{T_C N_{CH2}} \frac{\lambda}{1 - e^{-\lambda t}} = \frac{N_{C11}}{T_C} \frac{\lambda}{1 - e^{-\lambda t}} \left(\frac{N_P}{N_{CH2}}\right) \frac{1}{N_P} \quad (5)$$

where N_{C11} is the experimentally measured number of ^{11}C nuclei and N_P is the experimentally measured number of protons in the proton telescope, which was measured to less than 1% statistical uncertainty. The ratio N_{CH2}/N_P is given by Equation (3) in this simple approximate model. A similar result is obtained for the graphite target.

To determine the number of ^{11}C nuclei (N_{C11}), the targets were taken to the counting stations, and the number of ^{11}C decays in each was counted. The growth curve for ^{11}B from the positron decay of ^{11}C was determined by integrating the number of counts in one minute wide bins, each bin corrected for dead time. A fit of the growth function

$$R(t) = R_0\left(1 - e^{-\lambda t}\right) + At + B \quad (6)$$

to the measured ^{11}B growth curve, where R_0 is the final total number of ^{11}C decays detected, λ is the decay constant for ^{11}C, and A and B are background constants. This value was then corrected for the delay time between when the neutron irradiation ended and when decay counting began. Finally, the total number of ^{11}C present when the neutron bombardment ended (N_{C11}) was determined using the efficiencies of Table 1.

Figure 13 shows a typical ^{11}B growth curve. The measured data are clearly in excellent agreement with theory, and can be used to calculate the number of ^{11}C nuclei produced in the graphite by the ^{12}C(n, 2n)^{11}C reaction to within about 2-4%.

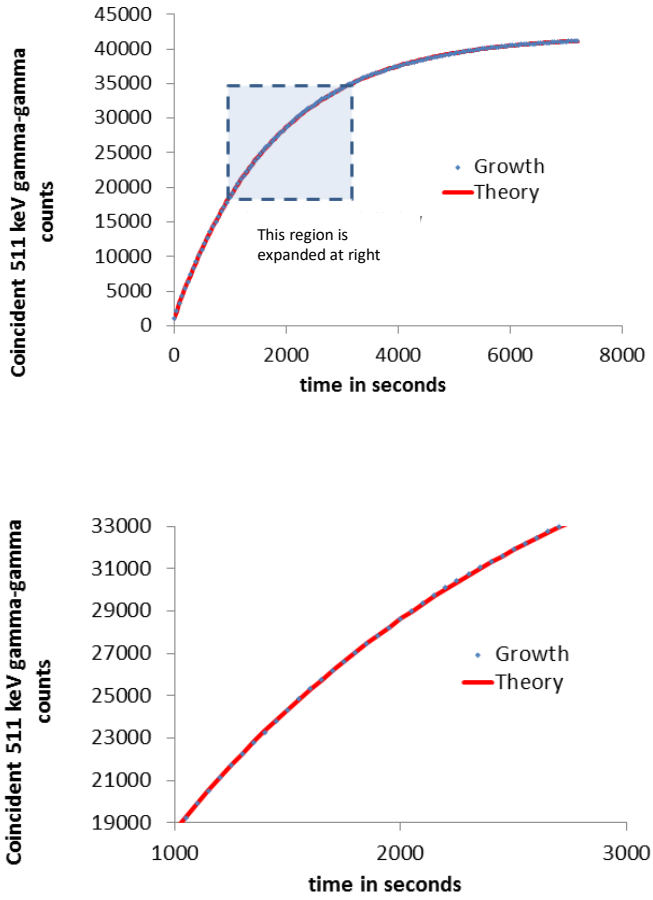

Figure 13. An ^{11}B growth curve (top). This curve indicates the number of newly created $_{11}$B nuclei from the decay of ^{11}C. The counted number of ^{11}B (blue) agrees well with the predicted number (red). The expanded region from 1,000 to 3,000 seconds (bottom) shows the excellent agreement between theory and measurement.

Clearly, the approximation that the tritium and CH_2 targets can be treated as point sources is incorrect, and a more correct approximation must include the fact that the neutrons leaving the tritium target can have a range of angles and still reach the CH_2 and graphite targets, and that the energies and cross sections for these neutrons depends on the neutron

angle. Moreover, the protons coming from the CH_2, which is an extended target, can also have a range of angles and still strike the proton telescope, and the cross sections and energies of the protons reaching the telescope depends on the proton angle.

In order to correct for these effects, the plastic and tritium target as well as the proton detector can be divided into differential area elements, and the ratio N_{CH2}/N_P calculated by integrating. This new ratio then can be used in Equation (5) for the ^{12}C(n, 2n) cross section.

In Figure 14, the surfaces of the tritium, plastic and graphite targets, as well as the dE detector in the proton telescope, are broken up into small area elements using cylindrical coordinates where the coordinates of the area elements are (r_i, θ_i) where $i = 1, 2, 3$ respectively. F_D is the deuteron flux through the tritium target, and E is the energy of these deuterons. The angles ϕ_1 and ϕ_2 are between the incident beam direction normal to the surfaces and the direction of the neutrons from the tritium target and the protons from the polyethylene target, respectively. E_1 and E_2 are the energies of the outgoing neutrons and protons, respectively. Distances R_1 and R_2, respectively, are the distance travelled by a neutron from the tritium target to the CH_2 target and the distance travelled by a proton from the CH_2 target to the detector.

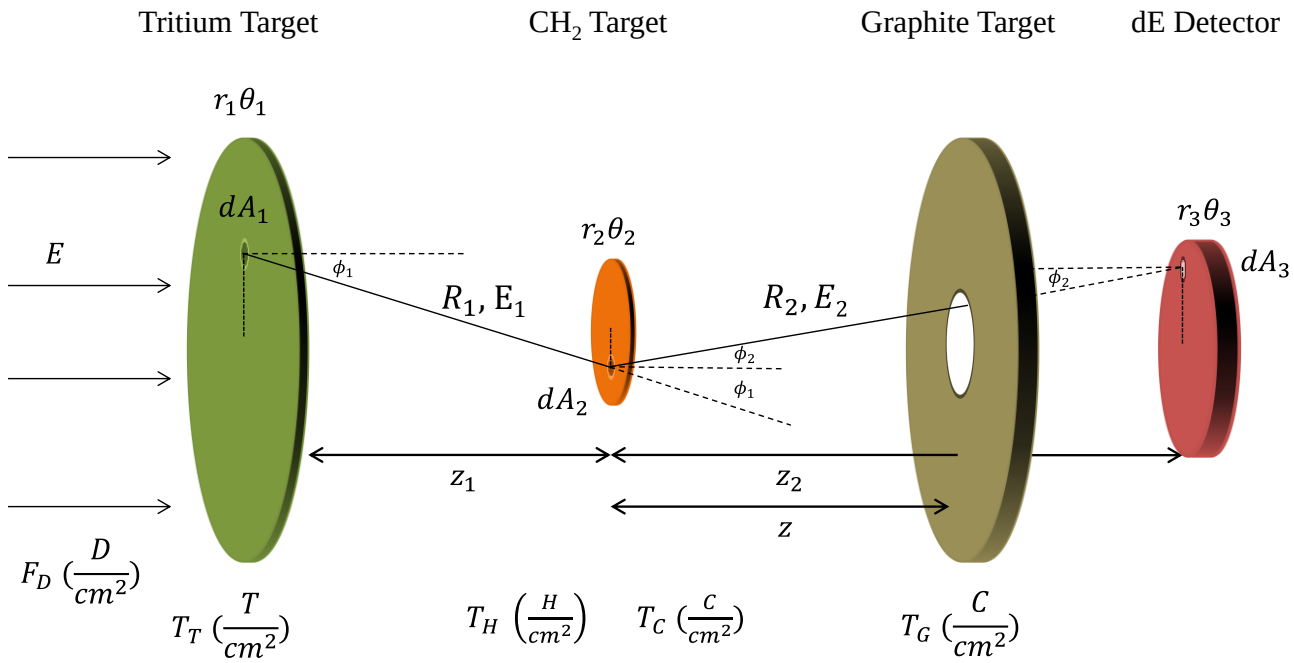

Figure 14. In order to calculate a better value for the ratio $\boldsymbol{N_{CH2}/N_P}$ the targets can be divided into infinitesimal area elements and the number of neutrons and protons from each element scattered into another element can be integrated.

Consider the infinitesimal number of neutrons dN_n leaving dA_1 at angle ϕ_1 and energy E_1,

$$\boldsymbol{dN_n = \sigma_{DT}(\phi_1, E)\, F_D\, T_T\, dA_1}\ . \qquad (7)$$

Integration of dN_n over the tritium and polyethylene targets then yields the total number of neutrons striking the surface of the CH_2 target

$$\boldsymbol{N_{CH2} = \int_{trit}\int_{CH_2} \sigma_{DT}(\phi_1, E)\, F_D\, T_T\, dA_1 d\Omega_2} \qquad (8)$$

where the infinitesimal solid-angle element $d\Omega_2$ for the polyethylene target is defined to be

$$\boldsymbol{d\Omega_2} = \frac{\vec{\boldsymbol{r}} \cdot \hat{\boldsymbol{n}} \boldsymbol{ds}}{\boldsymbol{r^3}} = \frac{\boldsymbol{R_1 \cos \phi_1 dA_2}}{\boldsymbol{{R_1}^3}} = \frac{\boldsymbol{\cos \phi_1 \, dA_2}}{\boldsymbol{{R_1}^2}} \tag{9}$$

giving

$$\boldsymbol{N_{CH2}} = \int_0^{2\pi} \int_0^{R_{CH_2}} \int_0^{2\pi} \int_0^{R_T} \boldsymbol{\sigma_{DT}(\phi_1, E)\, F_D\, T_T} \frac{\boldsymbol{\cos \phi_1}}{\boldsymbol{{R_1}^2}} \, \boldsymbol{r_1\, dr_1\, d\theta_1\, r_2\, dr_2\, d\theta_2}. \tag{10}$$

In Equations (9) and (10) the distance R_1 is given by

$$\vec{\boldsymbol{R}}_{\boldsymbol{1}} = (\boldsymbol{x_2 - x_1})\hat{\boldsymbol{\imath}} + (\boldsymbol{y_2 - y_1})\hat{\boldsymbol{\jmath}} + \boldsymbol{z_2}\hat{\boldsymbol{k}} \tag{11}$$

and therefore

$$\boldsymbol{{R_1}^2} = \boldsymbol{{r_2}^2 + {r_1}^2 - 2 r_1 r_2 \cos\theta_1 \cos\theta_2 - 2 r_1 r_2 \sin\theta_1 \sin\theta_2 + {z_2}^2} \tag{12}$$

since

$$\boldsymbol{x_i = r_i \cos\theta_i \ \text{and}\ y_i = r_i \sin\theta_i}\,. \tag{13}$$

The angle ϕ_1 is given by

$$\boldsymbol{\phi_1} = \boldsymbol{\cos^{-1}} \frac{\vec{\boldsymbol{R}}_{\boldsymbol{1}} \cdot \hat{\boldsymbol{k}}}{\boldsymbol{R_1}} = \boldsymbol{\cos^{-1}} \frac{\boldsymbol{z_2}}{\boldsymbol{R_1}}. \tag{14}$$

The number of neutrons striking the graphite target is found similarly, except that in this case the integral in Equation (10) starts at the inner radius of the hole in the graphite.

The infinitesimal element of the number of protons that travel from the CH_2 target to the detector is obtained by integrating dN_p, the number of protons that travel from the area element on the polyethylene target to the area element on the detector. To do this, the np cross section at angle $\psi = \phi_1 + \phi_2$ and energy E_1 is required

$$\boldsymbol{dN_p} = \boldsymbol{\sigma_{np}}\big(\boldsymbol{\psi, E_1(\phi_1)}\big)\, \boldsymbol{dN_n\, d\Omega_2} \frac{\boldsymbol{T_H}}{\boldsymbol{\cos \phi_1}} \boldsymbol{d\Omega_3} \tag{15}$$

Or, using Equation (10),

$$\boldsymbol{dN_p} = \boldsymbol{\sigma_{np}}\big(\boldsymbol{\psi, E_1(\phi_1)}\big)\, \boldsymbol{\sigma_{DT}(\phi_1, E)\, F_D\, T_T\, dA_1\, d\Omega_2} \, \frac{\boldsymbol{T_H}}{\boldsymbol{\cos \phi_1}} \, \boldsymbol{d\Omega_3}\,. \tag{16}$$

This can be integrated over all three surfaces to give the total number of protons striking the dE detector,

$$\boldsymbol{N_p} = \int_{\boldsymbol{det}} \int_{\boldsymbol{CH_2}} \int_{\boldsymbol{trit}} \boldsymbol{\sigma_{DT}(\phi_1, E)\, \sigma_{np}(\psi, E_1) F_D T_T} \frac{\boldsymbol{T_H}}{\boldsymbol{\cos \phi_1}} \boldsymbol{dA_1 d\Omega_2 d\Omega_3} \tag{17}$$

$$= \int_0^{2\pi} \int_0^{R_D} \int_0^{2\pi} \int_0^{R_{CH_2}} \int_0^{2\pi} \int_0^{R_T} \sigma_{DT}(\phi_1, E)\, \sigma_{np}(\psi, E_1)\, F_D\, T_T \, \frac{T_H}{\cos\phi_1} \, \frac{\cos\phi_2}{{R_2}^2} \, \frac{\cos\phi_1}{{R_1}^2} \, r_1 dr_1 d\theta_1 \, r_2 dr_2 d\theta_2 \, . r_3 dr_3 d\theta_3$$

The energy E_1 was calculated using non-relativistic energy and momentum conservation. The DT cross section $\sigma_{DT}(\phi_1, E)$ was integrated using a linear interpolation to the laboratory cross sections given by the computer code DROSG 2000 [8], and the np elastic scattering cross section was a linear

interpolation of the laboratory cross sections provided by the SAID database [9].

If the graphite disk is now added, as shown in Figure 14, its effect on the number of protons reaching the detector must be determined, because the graphite target blocks the path of some protons that are elastically scattered from the CH_2 target. To account for this, when Equation (17) was integrated, the computer program eliminated paths target from the integral that intersected the graphite. To do this, the distance $r(z)$ from the center for the proton path is determined by calculating the x and y coordinates along the path using the equation of a line. The slope in each direction is

$$\boldsymbol{m_x = \frac{x_3 - x_2}{z_2}} \textbf{ and } \boldsymbol{m_y = \frac{y_3 - y_2}{z_2}} \qquad (18)$$

and therefore

$$\boldsymbol{x(z) = m_x z + x_2} \textbf{ and } \boldsymbol{y(z) = m_y z + y_2}. \qquad (19)$$

The radius of the proton path at the position z corresponding to the edges of the hole in the graphite is

$$\boldsymbol{r(z) = \sqrt{x(z)^2 + y(z)^2}}. \qquad (20)$$

Using the results of the integrals in Equations (10) and (17) the quantity N_{CH2}/N_P was calculated and this more accurate ratio was used in Equation (5) to give the cross section.

The plots in Figures Figure 15 through Figure 17 show the angle and energy distributions obtained using the integrals above for the sizes and distances of the target and detectors used in this experiment. The angular distributions for neutrons striking the polyethylene target peaks at roughly 6° while the neutrons striking the graphite peak at about 12°, as one would expect since the solid angle is larger for the graphite and neutrons hitting the center hole do not count toward the integral. The scattering angle for np elastic scattering peaks at around 10°.

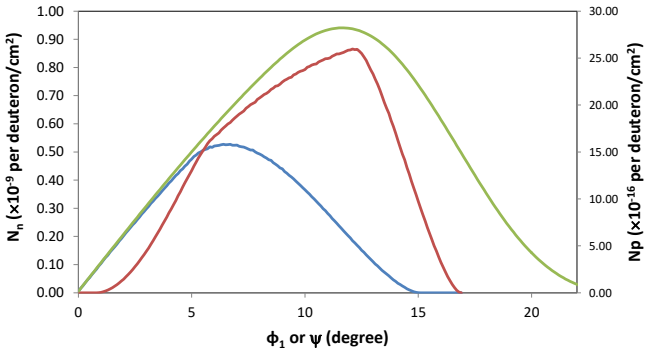

Figure 15. Plot of number of neutrons striking graphite (red) and polyethylene (blue) targets (left scale) as a function of ϕ_1, and number of protons striking the dE detector (green) (right scale) as a function of $\boldsymbol{\psi = \phi_1 + \phi_2}$ for 9 MeV deuterons hitting the tritium target.

Figure 16 shows the expected energy distribution of neutrons hitting the polyethylene and graphite targets. The average neutron energy for the polyethylene is lightly higher than for the graphite, as would be expected given that the angle is on average smaller, and that the DT cross section falls with angle. The range of neutron energies is about 0.5 MeV as predicted by simply considering the maximum possible angles. The calculation above does not include deuteron energy loss in the tritium target. However, deuterons in the tritium target will lose at most a few hundred keV.

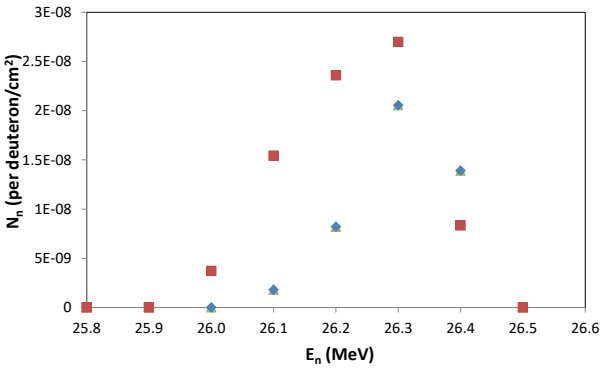

Figure 16. The energy distribution of neutrons hitting graphite (red squares) and polyethylene (blue diamonds) targets for 9 MeV deuterons hitting the tritium target.

The energy distribution for protons hitting the dE detector is plotted in Figure 17. The energy distribution has a peak near the maximum neutron energy of 26.4 MeV for 9 MeV deuterons hitting the tritium target. It falls to zero for protons with energies below about 22 MeV. Remember however

that this energy distribution does not include straggling or the energy loss of the protons passing through the polyethylene target, which should be about 5 MeV at 26.5 MeV.

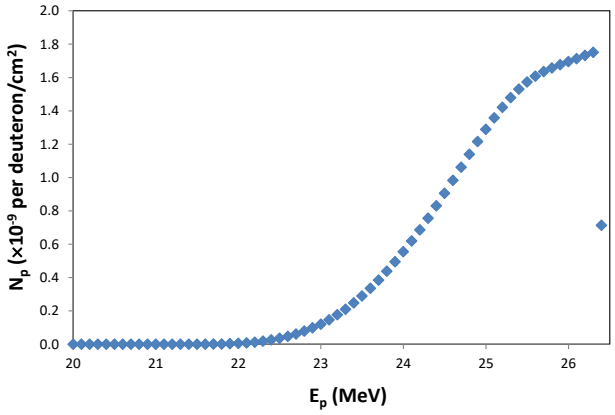

Figure 17. The energy distribution of protons hitting the dE target for 9 MeV deuterons hitting the tritium target. The energy loss and straggling of protons leaving the polyethylene target is not included.

Figure 18 shows the predicted ratios for N_{CH2}/N_P determined by using the simple point source model (Equation (3)) and the integral formulas. The largest difference between the simple model using point sources and the integral solution is at the highest energies, and is approximately 8%.

Finally, this analysis does not correct for the fact that the neutrons striking the targets, as shown in Figure 16, are not monoenergetic. In the analysis, it is assumed that the ^{12}C(n, 2n) cross section is being measured at $E_1(\phi_1 = 0°)$. To correct for this, it

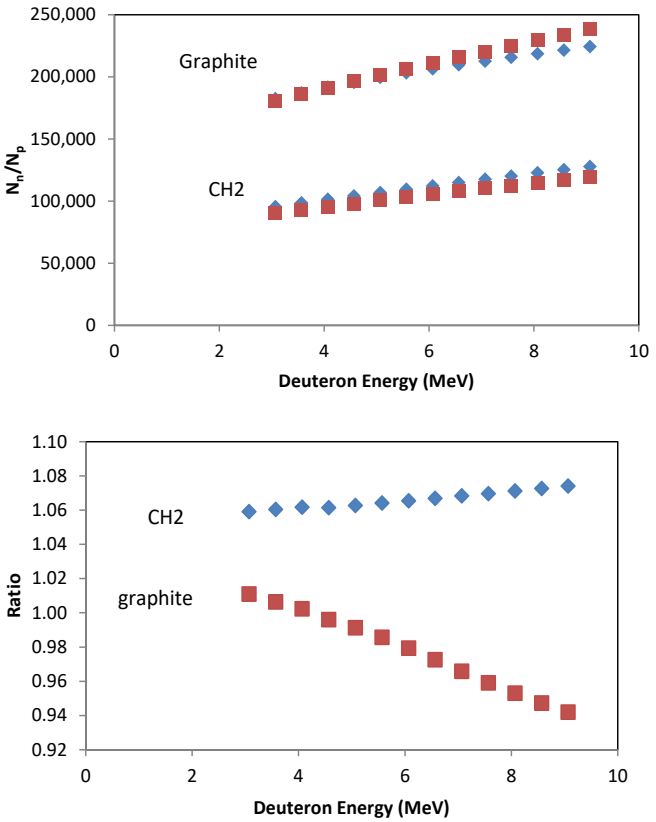

Figure 18. (Left) Plot of the ratio of the number of neutrons striking the CH_2 target (lower) and graphite target (upper) to the number of neutrons detected in the dE detector for the simple model of Equation (3) (red squares) and the integral solution of Equations (10) and (17) (blue diamonds). (Right) The ratio of the integral solution of Equations (10) and (17) to the simple model of Equation (3) for the CH_2 target (blue diamonds) and the graphite target (red squares).

should be possible to make use of Equations (4) and (7) calculate the number of ^{11}C nuclei

$$\frac{dN_{C11}}{dt} = \int \sigma T_C \frac{dN_n}{dt} - \lambda N_{C11} \tag{21}$$

$$= \int_{trit} \int_{G} \sigma_{DT}(\phi_1, E)\, F_D\, T_T \sigma\big(E_1(\phi_1)\big) \frac{T_C}{\cos\phi_1} dA_1\, d\Omega_2$$

$$= \int_0^{2\pi} \int_0^{R_T} \int_0^{2\pi} \int_0^{R_{CH_2}} \sigma_{DT}(\phi_1, E)\, \frac{F_D\, T_T\, T_C}{\cos\phi_1} \sigma(E_1(\phi_1))\, \frac{\cos\phi_1}{{R_2}^2}\, r_2\, dr_2\, d\theta_2\, r_1\, dr_1\, d\theta_1$$

Using the approximate value for the ^{12}C(n, 2n) cross section σ from previous measurements will allow a correction to be calculated to N_{CH2}/N_P obtained using Equations (10) and (17). This correction could then be applied to Equation (5) to obtain the cross section. One might expect this correction to be

rather small, however, since the $^{12}C(n, 2n)$ cross section does not appear to vary rapidly and the neutron distribution from Figure 16 only spans about 0.5 MeV.

Finally, it should be possible to check these calculations using MCNPX. Unfortunately, it seems the standard MCNPX cross section libraries do not include np elastic scattering cross sections for energies above 20 MeV, and may not properly handle the angular dependence of the cross section. Solutions to this problem are being explored.

FUTURE PLANS

Cross sections for the $^{12}C(n, 2n)$ reaction are needed for the range of energies spanned by tertiary neutrons from inertial confinement fusion. The facilities at Ohio University only allow measurements to be made up to a maximum neutron energy of 26.5 MeV. The possibility is being explored of making further measurements next summer at higher energies using neutrons produced by the 88-inch cyclotron at U.C. Berkeley.

PRESENTATIONS

Garrett Hartshaw, Keith Mann, Tyler Reynolds, Mark Yuly, Stephen Padalino, Danae Polsin, Megan Russ, Michael Krieger, Collin Stillman, Angela Simone, Mollie Bienstock, Drew Ellison, and Craig Sangster, "Measuring the Cross Section of the 12C(n,2n)11C Reaction for the 20-30MeV Energy Interval", XXXII Annual Rochester Symposium for Physics Students, University of Rochester, Rochester, NY., April 6, 2013.

Stephen Padalino, Danae Polsin, Megan Russ, Michael Krieger, Collin Stillman, Angela Simone, Mollie Bienstock, Drew Ellison, Mark Yuly, Keith Mann, Tyler Reynolds, Craig Sangster, "Cross Section of the (n, 2n) Reaction in 12C in the Energy Interval 20-30 MeV," 2012 Fall Meeting of the APS Division of Nuclear Physics, Newport Beach, CA, October 24-27, 2012.

Stephen Padalino, Danae Polsin, Megan Russ, Michael Krieger, Collin Stillman, Angela Simone, Mollie Bienstock, Drew Ellison, Mark Yuly, Keith Mann, Tyler Reynolds, Craig Sangster, "Coincidence Efficiency Measurement Using 11B(p,n)11C," 2012 Fall Meeting of the APS Division of Nuclear Physics, Newport Beach, CA, October 24-27, 2012.

Stephen Padalino, Danae Polsin, Megan Russ, Michael Krieger, Collin Stillman, Angela Simone, Mollie Bienstock, Drew Ellison, Mark Yuly, Keith Mann, Tyler Reynolds, Craig Sangster, "In Situ Calibration of a Proton Particle Telescope using the SUNY Geneseo 1.7 MV Tandem Pelletron Accelerator," 2012 Fall Meeting of the APS Division of Nuclear Physics, Newport Beach, CA, October 24-27, 2012.

Stephen Padalino, Danae Polsin, Megan Russ, Michael Krieger, Collin Stillman, Angela Simone, Mollie Bienstock, Drew Ellison, Mark Yuly, Keith Mann, Tyler Reynolds, Craig Sangster, "Cross Section of the (n, 2n) Reaction in 12C in the Energy Interval 20-30 MeV," 2012 Fall Meeting of the APS Division of Nuclear Physics, Newport Beach, CA, October 24-27, 2012.

This material is based upon work supported by the Department of Energy [National Nuclear Security Administration] University of Rochester "National Inertial Confinement Program" under Award Number(s) DE-NA0004144.

name, trademark, manufacturer, or otherwise does not necessarily constitute or imply its endorsement, recommendation, or favoring by the United States Government or any agency thereof. The views and opinions of authors expressed herein do not necessarily state or reflect those of the United States Government or any agency thereof.

REFERENCES

[1]. P. J. Dimbylow, Phys. Med. Biol. **25**, 637 (1980).
[2]. B. Anders et al., Zeit. Phys. A **301**, 353 (1981).
[3]. P. Welch et al., Bull. Am. Phys. Soc. **26**, 708 (1981).
[4]. O. D. Brill et al., Dok. Akad. Nauk SSR **136**, 55 (1961); F. Nasyrov et al., At. Energ**. 25**, 437 (1968).
[5]. T. S. Soewarsono et al., JAERI Tokai Rep. **27,** 354 (1992).
[6]. Uno et al., Nucl. Sci. Eng. **122**, 247 (1996); E. Kim et al., **129**, 209 (1998).
[7]. J. E. Brolley Jr. et al., Phys. Rev. **88**, 618 (1952).
[8]. M. Drosg, "DROSG-2000: Neutron Source Reactions," International Atomic Energy Agency Nuclear Data Services Report IAEA-NDS-87 (2000).
[9]. R.A. Arndt, I.I. Strakovsky, R.L. Workman, Phys. Rev. C **62,** 034005 (2000); R. A. Arndt et. al., Phys Rev. D **28**, 97 (1983).